Chapter 1
Time-Optimal Path Planning Along Specified Trajectories

Francisco Geu Flores and Andrés Kecskeméthy

Abstract Time-optimal motion planning along specified paths is a well-understood problem in robotics, for which well-established methods exist for some standard effects, such as actuator force limits, maximal path velocity, or sliding friction. This paper describes some extensions of the classical methods which consider, on the one hand side, additional non linear constraints such as sticking friction, acceleration limits at the end-effector, as well power limits for the overall system, and on the other, general paths featuring smooth interpolation of angular acceleration as well as arbitrary multibody systems comprising multiple loops. The methods are illustrated with two applications from robotics and the mining industry.

1.1 Introduction

The problem of computing the time-optimal motion of a manipulator along a prescribed spatial path under forces, velocities and acceleration constraints has been thoroughly studied in the past. The basic idea of most solution algorithms is based on the pioneer work by Dubowsky, Bobrow and Gibson [1] as well as Shin and McKay [7], and the modifications proposed by Pfeiffer and Johanni [5] and Shiller and Lu [6]. It consists in mapping both the multibody differential equations and the system constraints to a one-dimensional motion along the prescribed path in order to define the maximally allowed accelerations at each point on the path, and to seek, by means of forwards and backwards integrations, the optimal set of points where the optimal acceleration must switch from a maximum to a minimum or *vice versa*.

F. Geu Flores (✉) • A. Kecskeméthy
Universität Duisburg-Essen, Lotharstr. 1, Duisburg 47057, Germany
e-mail: francisco.geu@uni-due.de; andres.kecskemethy@uni-due.de

H. Gattringer and J. Gerstmayr (eds.), *Multibody System Dynamics, Robotics and Control*,
DOI 10.1007/978-3-7091-1289-2_1,

Messner, Gattringer and Bremer [4] extend these ideas to handle jerk constraints. Moreover, by applying methods of optimal control, they avoid searching for the switching points with backwards and forwards integrations, thus rendering very efficient, online-suitable code. However, their method is restricted to non-singular arcs, as well as systems for which the state of vanishing velocity is always feasible, thus limiting both search space and application domain. Although such cases are very special, they do happen in practice, two corresponding examples being shown in this paper.

A further recent approach is the reformulation of the problem as a convex optimal control problem by Verscheure, Demeulenaere, Swevers, De Schutter and Diehl [9]. This approach yields a very efficient and stable offline procedure. However, by considering only constraints that are linear in $\ddot{s}$ and $\dot{s}^2$, the application domain is additionally limited with respect to [7].

In summary, research on optimal-time path planning can be viewed as being focused on two directions. One is to develop new time-optimal algorithms as a basis for finding time-optimal paths between two configurations. In this setting, the aforementioned motion planning algorithm is used as an internal loop for computing the minimal-time motion after each path geometry variation. The second direction is to extend the systems for which time-optimal motion planning can be performed, both from the viewpoint of the multibody modeling as well as from the viewpoint of the regarded constraints.

This paper considers the second aim, extending the robotic modeling environment to arbitrary multiloop systems with general rigid-body motion interpolation options, as well as by adding sticking friction and global power limits to the set of allowable constraints. This allows for applying the method to a broader set of industrial problems and for easily generating the constraints of the path-planning algorithm regardless of the complexity of the kinematical structure. For motion interpolation along a prescribed path, we consider both interpolation along the spatial path between key poses of the end-effector (including smooth angular acceleration interpolation) as well as interpolation in generalized-coordinates (i.e. joint space), between which the user can switch. The flexibility of the method is shown by means of two examples in the mining industry and the field of robotics respectively. Further papers will consider the optimization of path geometry.

1.2 Spatial Paths in Multibody Systems

1.2.1 Kinetostatic Transmission Elements

A mechanical system can be regarded as a sequence of kinetostatic transmission elements mapping motion and forces from one set of state objects — the ‘input’ variables $\underline{q}_{\text{in}}$ — to another set of state objects — the ‘output’ variables $\underline{q}_{\text{out}}$ ([3]).

These state objects can be spatial reference frames and/or scalar variables, including associated velocities, accelerations and generalized forces.

The overall transmission behavior of a kinetostatic transmission element comprises a motion transmission traversal consisting of the three sub-operations

$$\begin{aligned} &\underline{\text{position}}: \quad \underline{q}_{\text{out}} = \varphi(\underline{q}_{\text{in}}) \\ &\underline{\text{velocity}}: \quad \dot{\underline{q}}_{\text{out}} = \mathbf{J}_\varphi \, \dot{\underline{q}}_{\text{in}} \\ &\underline{\text{acceleration}}: \ \ddot{\underline{q}}_{\text{out}} = \mathbf{J}_\varphi \, \ddot{\underline{q}}_{\text{in}} + \dot{\mathbf{J}}_\varphi \, \dot{\underline{q}}_{\text{in}} \end{aligned} \tag{1.1}$$

where $\mathbf{J}_\varphi = \partial\varphi/\partial\underline{q}_{\text{in}}$ represents the Jacobian of the element, as well as force transmission traversal consisting, for ideal transmission elements, of the sub-operation:

$$\underline{\text{force}}: \quad \underline{Q}_{\text{in}} = \mathbf{J}_\varphi{}^{\text{T}} \underline{Q}_{\text{out}}. \tag{1.2}$$

Any (passive) physical or mathematical object that maps a set of input state objects to a set of output state objects without loss or increase of mechanical power can be regarded as a kinetostatic transmission element.

1.2.2 Spatial Motion Parametrization

Let a general spatial path be given by the pose of an output frame $\mathcal{K}_{\text{E}} = \mathcal{P}(s) \in \text{SE}(3)$, with the translation part parametrized by vector $\Delta\underline{r}(s)$ and the rotation part described by a rotation matrix $\Delta\mathbf{R}(s)$, both measured with respect to a basis frame $\mathcal{K}_1$. Let the coordinate s be the path length of $\Delta\underline{r}(s)$. The spatial path $\mathcal{P}(s)$ can be modelled as a kinetostatic transmission element mapping the velocity $\dot{s}$ along the path to the end-effector twist $\underline{\text{t}}_{\text{E}}$ and, by duality, the wrench $\underline{\text{w}}_{\text{E}}$ acting at the end-effector to a generalized force Q_s along the path, as shown in Fig. 1.1.

The pose of $\mathcal{K}_{\text{E}}$ can be computed as a function of the pose of the basis frame $\mathcal{K}_1$ and the path coordinate s as

$$\begin{aligned} \mathbf{R}_{\text{E}} &= \mathbf{R}_1 \, \Delta\mathbf{R} \\ \underline{r}_{\text{E}} &= \Delta\mathbf{R}^{\text{T}}(\underline{r}_1 + \Delta\underline{r}), \end{aligned} \tag{1.3}$$

where general vectors are assumed to be decomposed in the target frame and $\mathbf{R}_i$ denotes the rotation matrix transforming coordinates with respect to frame $\mathcal{K}_i$ to coordinates with respect to frame $\mathcal{K}_0$.

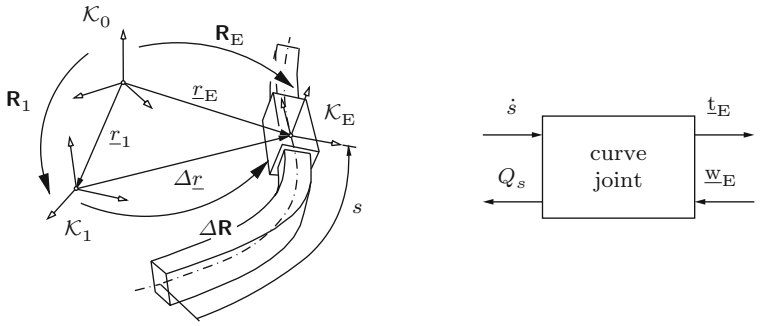

Fig. 1.1 Spatial joint as a kinetostatic transmission element

The velocity transmission then takes the form

$$\begin{bmatrix} \underline{\omega}_\mathrm{E} \\ \underline{v}_\mathrm{E} \end{bmatrix} = \mathbf{J}_g \begin{bmatrix} \underline{\omega}_1 \\ \underline{v}_1 \end{bmatrix} + \mathbf{J}_\mathcal{P}\,\dot{s}, \qquad \text{with} \quad \mathbf{J}_g = \begin{bmatrix} \Delta\mathbf{R}^\mathrm{T} & \underline{0} \\ -\Delta\mathbf{R}^\mathrm{T}\widetilde{\Delta\underline{r}} & \Delta\mathbf{R}^\mathrm{T} \end{bmatrix}, \tag{1.4}$$

where $\mathbf{J}_g$ is the rigid-body Jacobian, $\mathbf{J}_\mathcal{P}$ is the Jacobian mapping the path velocity $\dot{s}$ along the spatial path to the twist at the output frame $\mathcal{K}_\mathrm{E}$, and $\widetilde{\underline{a}}$ refers to the skew-symmetric matrix generated by a three-dimensional vector $\underline{a} = \begin{bmatrix} a_x\, a_y\, a_z \end{bmatrix}^\mathrm{T}$.

The acceleration transmission can be written as

$$\begin{bmatrix} \dot{\underline{\omega}}_\mathrm{E} \\ \underline{a}_\mathrm{E} \end{bmatrix} = \mathbf{J}_g \begin{bmatrix} \dot{\underline{\omega}}_1 \\ \underline{a}_1 \end{bmatrix} + \begin{bmatrix} \underline{0} \\ {}^2\tilde{\underline{\omega}}_1^2 \Delta\mathbf{R}^\mathrm{T}\Delta\underline{r} \end{bmatrix} + \mathbf{J}_\mathcal{P}\,\ddot{s} + \mathbf{J}_\mathcal{P}'\dot{s}^2 + \begin{bmatrix} {}^2\widetilde{\underline{\omega}}_1 & \mathbf{0} \\ \mathbf{0} & 2^2\widetilde{\underline{\omega}}_1 \end{bmatrix} \mathbf{J}_\mathcal{P}\,\dot{s}, \tag{1.5}$$

where $(.)'$ denotes a derivative with respect to the path coordinate s.

According to Eq. 1.2, the force transmission yields

$$\begin{bmatrix} \underline{\tau}_1 \\ \underline{f}_1 \\ Q_s \end{bmatrix} = \begin{bmatrix} \mathbf{J}_g^\mathrm{T} \\ \mathbf{J}_\mathcal{P}{}^\mathrm{T} \end{bmatrix} \begin{bmatrix} \underline{\tau}_\mathrm{E} \\ \underline{f}_\mathrm{E} \end{bmatrix}. \tag{1.6}$$

A complete description on how $\Delta\underline{r}(s)$ and $\Delta\mathbf{R}(s)$ can be defined can be found in [8]. In the examples presented in this paper, the function $\Delta\underline{r}(s)$ is obtained by interpolating key poses with quintic B-splines, using the DIERCKX curve-fitting routines [2] with prescribed boundary conditions for positions, tangents and curvature. The orientation $\Delta\mathbf{R}(s)$ of the output frame along the curve is then prescribed as a function of the geometry of the curve $\Delta\underline{r}(s)$ and additional elementary rotations with respect to the natural directions of the curve, prescribed as cubic B-spline functions of

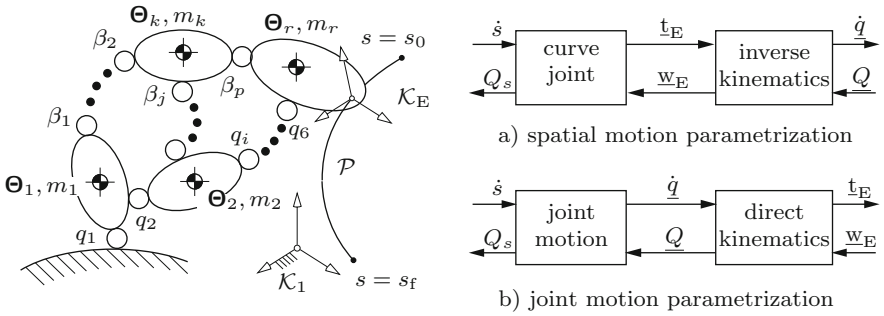

Fig. 1.2 Motion parametrization using (**a**) target coord. or (**b**) joint coord

the path coordinate s. Nevertheless, these equations also hold for more general path parametrizations.

Let $\underline{\varphi}_q$ be the direct kinematics of the manipulator with n degrees of freedom with serial or closed kinematical topology, described by n independent joint coordinates q_i, collected in the vector $\underline{q} \in \mathbb{R}^n$. If the spatial path $\mathcal{P}(s)$ of the end-effector is contained in its workspace, the system can be understood as a closed chain with one degree of freedom, as shown in Fig. 1.2a. The corresponding joint motion is, hence, described by the equations

$$\begin{aligned} \underline{q} &= \underline{\varphi}_q{}^{-1}(\mathcal{P}(s)) \\ \dot{\underline{q}} &= \mathbf{J}_\varphi{}^{-1}\mathbf{J}_\mathcal{P}\dot{s} \\ \ddot{\underline{q}} &= \mathbf{J}_\varphi{}^{-1}\mathbf{J}_\mathcal{P}\ddot{s} + \left[\mathbf{J}'_\varphi{}^{-1}\mathbf{J}_\mathcal{P} + \mathbf{J}_\varphi{}^{-1}\mathbf{J}'_\mathcal{P}\right]\dot{s}^2, \end{aligned} \tag{1.7}$$

where $\mathbf{J}_\varphi = \partial\underline{\varphi}_q / \partial\underline{q}$ represents the transmission Jacobian of the manipulator.

1.2.3 Joint Motion Parametrization

For some applications where the interpolated pose of the end-effector does not have to fulfill any geometrical constraints along the given spatial path, or for the special case of manipulators with limited degrees of freedom, the interpolation of motion in joint coordinates can be of advantage. In these cases, the motion can be given as $\underline{q} = \underline{\eta}(s) \in \mathbb{R}^n$, which can also be represented as a kinetostatic transmission element mapping the motion progress, described by a motion coordinate $s(t)$ which is now not the path coordinate, to the joint motion $\underline{q}(t)$ and end-effector motion $\mathcal{K}_E(t)$, as shown in Fig. 1.2b.

In this case the corresponding end-effector motion is described by the equations

$$\begin{aligned} \mathcal{K}_{\mathrm{E}} &= \underline{\varphi}_q\big(\underline{\eta}(s)\big) \\ \mathrm{t}_{\mathrm{E}} &= \mathbf{J}_\varphi \mathbf{J}_\eta \dot{s} \\ \dot{\mathrm{t}}_{\mathrm{E}} &= \mathbf{J}_\varphi \mathbf{J}_\eta \ddot{s} + \left[\mathbf{J}_\varphi' \mathbf{J}_\eta + \mathbf{J}_\varphi' \mathbf{J}_\eta\right] \dot{s}^2, \end{aligned} \tag{1.8}$$

where $\mathbf{J}_\eta = \partial\underline{\eta}/\partial s$ represents the transmission Jacobian of $\underline{\eta}$ with respect to the motion coordinate s.

For both cases described above, the velocities and accelerations at the independent manipulator joints and the end-effector have the general form

$$\begin{aligned} \dot{\underline{q}} &= {}_q\mathbf{J}_s\, \dot{s}: & \underline{\mathrm{t}}_{\mathrm{E}} &= {}_{\mathrm{E}}\mathbf{J}_s\, \dot{s}, \\ \ddot{\underline{q}} &= {}_q\mathbf{J}_s\, \ddot{s} + {}_q\mathbf{J}_s'\, \dot{s}: & \dot{\underline{\mathrm{t}}}_{\mathrm{E}} &= {}_{\mathrm{E}}\mathbf{J}_s\, \ddot{s} + {}_{\mathrm{E}}\mathbf{J}_s'\, \dot{s}. \end{aligned} \tag{1.9}$$

1.3 Time-Optimal Motion Generation

1.3.1 Formulation of the Time-Optimal Problem

Let the dynamics of a multibody system be described by the differential equations in minimal form

$$\mathbf{M}(\underline{q})\ddot{\underline{q}} + \underline{b}(\underline{q}, \dot{\underline{q}}) + \underline{Q}_{\mathrm{e}}(\underline{q}, \dot{\underline{q}}) + \underline{Q}_{\mathrm{G}}(\underline{q}) = -\underline{Q}, \tag{1.10}$$

where $\mathbf{M}$ is the $n \times n$ mass matrix of the multibody system, $\underline{b}(\underline{q}, \dot{\underline{q}})$ is the n-dimensional vector containing the centripetal and Coriolis terms, $\underline{Q}_{\mathrm{G}}(\underline{q})$ is an n-dimensional vector containing the projection of the gravitational forces on the generalized coordinates, $\underline{Q}_{\mathrm{e}}(\underline{q}, \dot{\underline{q}})$ is an n-dimensional vector containing the projection of general external forces, and $\underline{Q}$ is an n-dimensional vector collecting the generalized actuator forces.

Let the velocities $\dot{\underline{q}}$, accelerations $\ddot{\underline{q}}$, and generalized actuator forces $\underline{Q}$ at the joints be constrained by equations of the form

$$\begin{aligned} \dot{\underline{q}}^{\min}\left(\underline{q}\right) &\le \dot{\underline{q}} \le \dot{\underline{q}}^{\max}(\underline{q}) \\ \ddot{\underline{q}}^{\min}(\underline{q}, \dot{\underline{q}}) &\le \ddot{\underline{q}} \le \ddot{\underline{q}}^{\max}(\underline{q}, \dot{\underline{q}}) \\ \underline{Q}^{\min}(\underline{q}, \dot{\underline{q}}) &\le \underline{Q} \le \underline{Q}^{\max}(\underline{q}, \dot{\underline{q}}), \end{aligned} \tag{1.11}$$

and the velocities $\underline{\mathrm{t}}_{\mathrm{E}}$ and accelerations $\dot{\underline{\mathrm{t}}}_{\mathrm{E}}$ at the end-effector be constrained by equations of the form

$$\begin{aligned} \underline{\mathrm{t}}_{\mathrm{E}}^{\min}(\mathcal{K}_{\mathrm{E}}) \leq \underline{\mathrm{t}}_{\mathrm{E}} \leq \underline{\mathrm{t}}_{\mathrm{E}}^{\max}(\mathcal{K}_{\mathrm{E}}) \\ \dot{\underline{\mathrm{t}}}_{\mathrm{E}}^{\min}(\mathcal{K}_{\mathrm{E}},\, \underline{\mathrm{t}}_{\mathrm{E}}) \leq \dot{\underline{\mathrm{t}}}_{\mathrm{E}} \leq \dot{\underline{\mathrm{t}}}_{\mathrm{E}}^{\max}(\mathcal{K}_{\mathrm{E}},\, \underline{\mathrm{t}}_{\mathrm{E}}). \end{aligned} \tag{1.12}$$

With the relations Eq. 1.9, the equations of motion described in Eq. 1.10 can be written in terms of the motion coordinate s as

$$\underline{m}(s)\ddot{s} + \underline{c}(s,\, \dot{s}) + \underline{d}(s) = -\underline{Q}, \tag{1.13}$$

with

$$\begin{aligned} \underline{m}(s) &= \mathbf{M}(s)\, {}_{q}\mathbf{J}_{s} \\ \underline{c}(s,\, \dot{s}) &= \left[\mathbf{M}(s)\, {}_{q}\mathbf{J}_{s}^{'} + \bar{\underline{b}}(s)\right]\, \dot{s}^2 + \underline{Q}_{\mathrm{e}}(s, \dot{s}) \\ \underline{d}(s) &= \underline{Q}_{\mathrm{G}}(s), \end{aligned} \tag{1.14}$$

where the coefficients m_i and c_i represent the effective inertia and velocity forces at every independent joint respectively, and the term $\underline{b}(\underline{q}, \dot{\underline{q}})$ in Eq. 1.10 can be written as $\bar{\underline{b}}(s)\, \dot{s}^2$, with $\bar{\underline{b}}(s)$ depending only on the configuration s.

Furthermore, Eq. 1.9 allows for all constraints of the form described in Eqs. 1.11 and 1.12 to be collected in the vector inequality

$$\hat{\underline{b}}_1(s, \dot{s}) \leq \hat{\underline{m}}(s)\, \ddot{s} \leq \hat{\underline{b}}_2(s, \dot{s}), \tag{1.15}$$

where $\hat{\underline{b}}_1$, $\hat{\underline{b}}_2$ and $\hat{\underline{m}}$ are vectors in $\mathbb{R}^l$ and l is the number of constraints.

The left and right terms of this inequality define the set of admissible states $[s,\, \dot{s}]^{\mathrm{T}}$ and can be written as the scalar inequality

$$g(s, \dot{s}) \leq 0, \tag{1.16}$$

with $g(s, \dot{s}) = \max\left\{\hat{b}_{1j}\ (s, \dot{s}) - \hat{b}_{2j}\ (s, \dot{s})\right\}$, for all $j = 1, 2, \cdots, \ell$.

For all constraints j for which $\hat{m}_j(s)$ does not vanish, Eq. 1.15 further limits the acceleration $\ddot{s}$ along the spatial path, since it must hold

$$\frac{\hat{b}_{1j}(s, \dot{s})}{|\hat{m}_j(s)|} \leq \operatorname{sgn}\left[\hat{m}_j(s)\right]\ddot{s} \leq \frac{\hat{b}_{2j}(s, \dot{s})}{|\hat{m}_j(s)|}, \tag{1.17}$$

or compactly

$$l_j(s, \dot{s}) \leq \ddot{s} \leq u_j(s, \dot{s}), \tag{1.18}$$

where $l_j(s,\dot{s})$ and $u_j(s,\dot{s})$ are the lower and upper bounds of the j-th constraint, functions of the state $[s,\dot{s}]^{\mathrm{T}}$. These equations can be rewritten as the one dimensional inequality

$$L(s,\dot{s}) \leq \ddot{s} \leq U(s,\dot{s}), \tag{1.19}$$

where $L(s,\dot{s}) = \max\{l_j(s,\dot{s})\}$ and $U(s,\dot{s}) = \min\{u_j(s,\dot{s})\}$ for all $j = 1,2,\cdots,\ell$ for which $\hat{m}_j(s) \neq 0$.

The time optimal problem consists in finding the monotonically increasing function $s(t)$ which minimizes the total time needed to travel from s_0 to s_f, without violating Eq. 1.19 or Eq. 1.16.

In this paper, further constraints that match Eq. 1.15 but are nonquadratically nonlinear in $\dot{s}$ are investigated. These stem from linear constraints at the end-effector accelerations in the form

$$|\mathbf{A}(\mathcal{K}_\mathrm{E})\,\dot{\underline{\mathrm{t}}}_\mathrm{E}(\mathcal{K}_\mathrm{E},\underline{\mathrm{t}}_\mathrm{E})| \leq \dot{\underline{\mathrm{t}}}_\mathrm{E}^{\max}, \tag{1.20}$$

where $\mathbf{A}(\mathcal{K}_\mathrm{E})$ is a 6×6 matrix depending on the manipulator configuration, as well as a limit for maximally allowed power consumption

$$|\underline{\dot{q}}^{\mathrm{T}}(\underline{q},\underline{\dot{q}})\underline{Q}(\underline{q},\underline{\dot{q}},\underline{\ddot{q}})| \leq P_{\max}. \tag{1.21}$$

1.3.2 Computation of the Dynamic Constraints

By using the object-oriented approach described in [3], the aforementioned dynamic constraints can be easily computed at every state $[s,\dot{s}]^{\mathrm{T}}$.

Let the transmission of motion from the motion coordinate s to the mass and force elements be given by a kinetostatic transmission element φ_S, denoted global kinematics. The concatenation of position, velocity, acceleration and force transmission functions of the global kinematics yields the inverse dynamics $\varphi_S^{D^{-1}}$ of the system, which maps the generalized coordinates and their time derivatives to a set of residual generalized forces

$$\underline{\bar{Q}} = \varphi_S^{D^{-1}}(s,\dot{s},\ddot{s}) = -\underline{m}(s)\,\ddot{s} - \underline{c}(s,\dot{s}) - \underline{d}(s), \tag{1.22}$$

at the input of the global kinematics. These residual forces can be used to generate $\underline{m}$, $\underline{c}$, and $\underline{d}$ of Eq. 1.13 at every configuration s by the following simplified procedure:

(a) Computation of $\underline{d}$: Set, at the input of $\varphi_S^{D^{-1}}$, the generalized velocities to $\dot{s} = 0$ and the generalized accelerations to $\ddot{s} = 0$. Then, the terms $\underline{m}\,\ddot{s}$ and $\underline{c}$ of Eq. 1.13 vanish and the residual vector obtained at the input is exactly $-\underline{d}$.

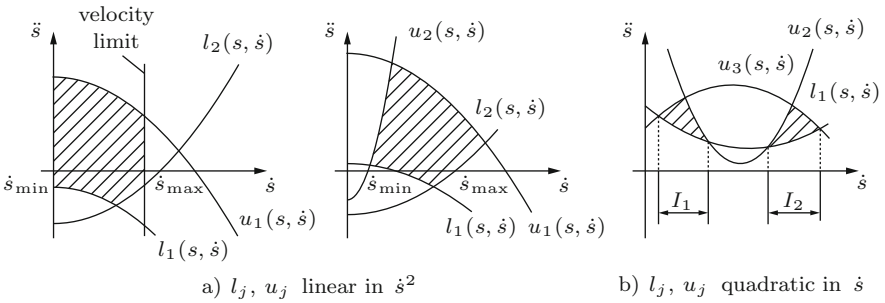

Fig. 1.3 Admissible acceleration region for given configuration s

(b) Computation of $\underline{c}$: Eliminate the term $\underline{d}$ in the calculation of $\varphi_S^{D^{-1}}$ by 'switching off' the gravitational forces $\underline{Q}_G$, and set, at the input of $\varphi_S^{D^{-1}}$, the generalized velocities to $\dot{s} = 1$ and the generalized accelerations to $\ddot{s} = 0$. Then, the term $\underline{m}\,\ddot{s}$ of Eq. 1.13 vanishes and the residual vector obtained at the input is exactly $-\underline{c}$.
(c) Computation of $\underline{m}$: Similarly, eliminate the term $\underline{d}$ in the calculation of $\varphi_S^{D^{-1}}$ and set the input acceleration to $\ddot{s} = 1$. Then, the resulting force $\bar{Q}$ is exactly $-\underline{m}$.

The Jacobian matrices can be computed similarly, using only the force transmission functions, as proposed by [3]. Consider a kinetostatic element such as the one defined in Sect. 1.2.1. Setting all force components at the output of the transmission element besides the jth-one equal to zero, and the jth-one equal to one, yields a vector of generalized forces at the input the transmission element which is identical to the jth-column of the transposed Jacobian, thus to its jth-row.

1.3.3 Solution of the Time-Optimal Problem

Equations 1.19 and 1.16 form a set of velocity and acceleration limits at every configuration s. These limits determine an admissible region in the plane $\dot{s} - \ddot{s}$ for each configuration s. Figure 1.3 shows typical admissible regions for two particular cases: (a) functions l_j, u_j linear in $\dot{s}^2$, and (b) functions l_j, u_j that are generally quadratic in $\dot{s}$. For the case of l_j, u_j linear in $\dot{s}^2$ one can define one simple interval $[\dot{s}_{\min}, \dot{s}_{\max}]$ of admissible velocities for every configuration s. This assumption is not valid in general, since the admissible region could consist of not connected subregions leading to a set not connected admissible velocity intervals (I_1, I_2 in Fig. 1.3b).

The time optimal problem becomes particularly simple if all constraints are linear in $\dot{s}^2$. In this case, constraint equations of the form Eq. 1.15 can be written as

$$\hat{\underline{c}}_1(s)\dot{s}^2 + \hat{\underline{d}}_1(s) \leq \hat{\underline{m}}(s)\,\ddot{s} \leq \hat{\underline{c}}_2(s)\dot{s}^2 + \hat{\underline{d}}_2(s) \tag{1.23}$$

The function $g(s,\dot{s})$ is linear in $\dot{s}^2$, which means that the admissible regions in the plane $\dot{s}-\ddot{s}$ are simply connected and the set of admissible states has no holes in its interior. This allows for the definition of the functions $\dot{s}_{\min}(s)$ and $\dot{s}_{\max}(s)$ describing the maximally and minimally allowed admissible velocities $\dot{s}$ as a function of the motion coordinate s.

In many applications, the lower limiting curve $\dot{s}_{\min}(s)$ is required to be zero along the whole spatial path, so that all multibody system configurations are feasible at rest. However it actually does not need to be so in order for the time-optimal problem to have a feasible solution, as shown in Sect. 1.4.2.

The states that lie on the upper limiting curve $\dot{s}_{\max}(s)$ are classified in:

(a) Sinks, if $U(s,\dot{s}) = L(s,\dot{s}) > \dot{s}_{\max}\ \mathrm{d}\dot{s}_{\max}/\mathrm{d}s$
(b) Source, if $U(s,\dot{s}) = L(s,\dot{s}) < \dot{s}_{\max}\ \mathrm{d}\dot{s}_{\max}/\mathrm{d}s$
(c) Tangent points, elsewhere.

Moreover, the tangent points at which the velocity constraints described in Eq. 1.16 are active are called singular points, or singular arcs if they are connected.

The solution to the time optimal motion is a sequence of branches of maximal accelerations and maximal decelerations that lies in the feasible region and touches tangentially the upper limiting curve. At states $[s,\dot{s}]^{\mathrm{T}}$ that lie inside the feasible region, the solution consists of segments with maximal acceleration $U(s,\dot{s})$ and segments with maximal deceleration $L(s,\dot{s})$. At singular points, the extremal accelerations are further bounded by the upper limiting curve tangent $\mathrm{d}\dot{s}_{\max}/\mathrm{d}s$.

With these definitions, the following algorithm based on the one proposed by [6] has been constructed:

Step 0: Check if the initial state s_0 and the final state s_{f} are feasible for the given initial velocity $\dot{s}_0$ and final velocity $\dot{s}_{\mathrm{f}}$ respectively. If not, the problem has no feasible solution.

Step 1: Set a counter k to 1. Integrate the equation $\ddot{s} = \max\{l_j(s,\dot{s})\}$ backwards in time from the final state $s = s_{\mathrm{f}}, \dot{s} = \dot{s}_{\mathrm{f}}$ until leaving the feasible region. Name the computed deceleration curve $\dot{s}^d(s)$.

Step 2: Integrate the equation $\ddot{s} = \min\{u_j(s,\dot{s})\}$ forwards in time from the initial state $s = s_0\ ,\ \ \dot{s} = \dot{s}_0$ until leaving the feasible region. Name the computed acceleration curve $\dot{s}^a_k(s)$. If the acceleration curve $\dot{s}^a_k(s)$ crosses the lower limiting curve $\dot{s}_{\min}(s)$, the problem is not feasible and the algorithm should be terminated. Else, continue.

Step 3: If $\dot{s}^a_k(s)$ crosses the deceleration curve $\dot{s}^d(s)$ terminate the algorithm: the intersection of both curves is the only switching point S_k. Otherwise, continue.

Step 4: Search forwards on the upper limiting curve $\dot{s}_{\max}(s)$ for the next tangency point S_{k+1}. The point S_{k+1} is a switching point candidate.

Step 5: Integrate the equation $\ddot{s} = \max\{l_j(s,\dot{s}), \dot{s}_{\max}\mathrm{d}\dot{s}_{\max}/\mathrm{d}s\}$ backwards in time from the state S_{k+1} until crossing one of the acceleration curves $\dot{s}^a_\ell(s)$, with $1 \le \ell \le k$. The intersection of both curves is the switching point S_ℓ. Set $k = \ell$. Disregard the candidates S_r, with $r \le \ell$.

Step 6: Integrate the equation $\ddot{s} = \min\{u_j(s,\dot{s}), \dot{s}_{\max}\,\mathrm{d}\dot{s}_{\max}/\mathrm{d}s\}$ forward in time from the state S_k until leaving the feasible region. Add one to the counter k. Name the

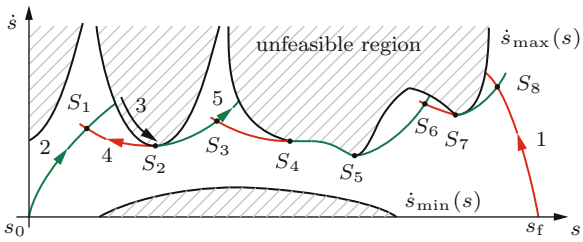

Fig. 1.4 Time-optimal solution algorithm (no islands)

computed acceleration curve $\dot{s}_k^a(s)$. If the acceleration curve $\dot{s}_k^a(s)$ crosses the lower limiting curve $\dot{s}_{\min}(s)$, the problem is not feasible and the algorithm should be terminated. Else, go to step (3).

Figure 1.4 shows how a typical solution looks like.

For more general functions l_j, u_j, the feasible region may be composed of several unconnected regions of admissibility. In this case, the computation of the set of admissible states requires the solution of the scalar inequality Eq. 1.16, which involves the search for the zeros of $g(s, \dot{s})$ for given configurations s. This is possible only if enough information on the nature of the nonlinearities is available, as in the example presented in Sect. 1.4.1. If this is the case, all tangent points on the boundary of the admissible states can be computed. This allows for the construction of a directed graph containing a set of trajectories which connect the tangent points with the initial and final states, the highest of which yields the time-optimal motion.

1.4 Application Examples

1.4.1 Loading Cycles of Backhoe Excavators

As a first example, consider the computation of the minimal time that an excavator would need to move along a typical load and haul path without violating the maximally allowed actuator forces as well as the maximally allowed overall hydraulic power consumption. A typical backhoe excavator consists of an under carriage, an upper carriage, a boom, a stick and a shovel (see Fig. 1.5). Its kinematical structure comprises three independent planar kinematical loops contained in the boom-stick plane as well as an independent rotation around a vertical axis.

The given path is interpolated in joint space using third order B-splines and it is assumed that the excavator starts its motion from and finishes it at rest. The dynamic constraints comprise the maximal hydraulic forces at the four actuators

$$Q_i^{\min} \leq \underline{Q} \leq Q_i^{\max}, \quad i = 1, 2, ..., 4, \tag{1.24}$$

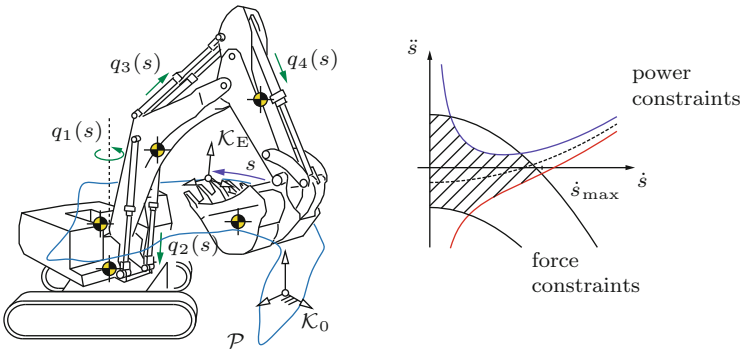

Fig. 1.5 Loading cycle of a backhoe excavator

which leads to constraint equations of the form Eq. 1.19 with functions $l_j(s,\dot{s}), u_j(s,\dot{s})$ linear in $\dot{s}^2$, as well as the maximal hydraulic power

$$|\dot{\underline{q}}^{\mathrm{T}}\underline{Q}| \leq P_{\max}, \tag{1.25}$$

which together with Eqs. 1.9, 1.13, and 1.14 leads to

$$\frac{-P_{\max}}{\hat{m}(s)\dot{s}} - \frac{\hat{b}(s,\dot{s})}{\hat{m}(s)} \leq \ddot{s} \leq \frac{P_{\max}}{\hat{m}(s)\dot{s}} - \frac{\hat{b}(s,\dot{s})}{\hat{m}(s)}: \tag{1.26}$$

with

$$\hat{m} = {}_q\mathbf{J}_s^{\mathrm{T}}\mathbf{M}(s)\,{}_q\mathbf{J}_s > 0 \tag{1.27}$$

$$\hat{b} = {}_q\mathbf{J}_s^{\mathrm{T}}[\mathrm{M}(s)\,{}_q\mathbf{J}_s' + \bar{\underline{b}}(s)]\dot{s}^2 + {}_q\mathbf{J}_s{}^{\mathrm{T}}\underline{Q}_{\mathrm{G}}(s). \tag{1.28}$$

In this case, the function $g(s,\dot{s})$ of Eq. 1.16 has, for a given configuration s, at the most three zeros, all of which can be computed exactly. The representation of the acceleration constraints in the $\ddot{s}-\dot{s}$ plane is shown in Fig. 1.5. The force constraints form parabolas with vertices on the $\ddot{s}$ axis, whereas the power constraints approach hyperbolically to a similar parabola.

The time optimal solution is plotted in Fig. 1.6. The plots show alternating horizontal plateaus which are to be seen through the different curves, which indicates that at least one of the maximally allowed forces or the maximal power consumption is always used.

1.4.2 Waiter-Motion Problem for a Given Spatial Path

As a second example, consider the so called "generalized waiter-motion problem". The well-known task consists in moving a tablet carrying a number of glasses from

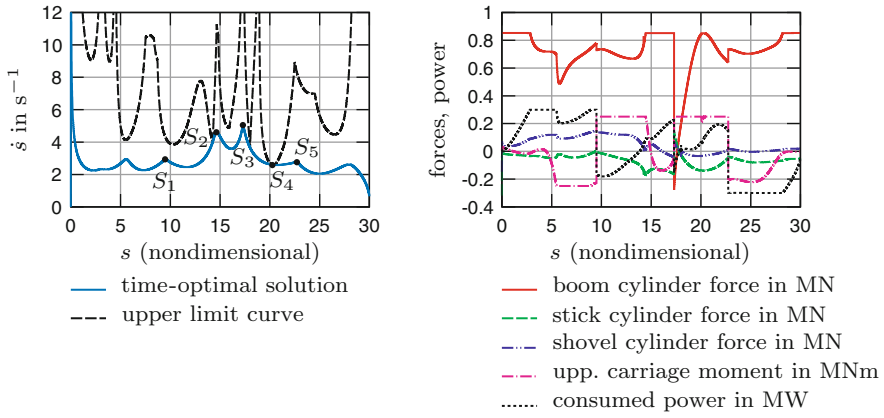

Fig. 1.6 Optimized backhoe excavator loading cycle

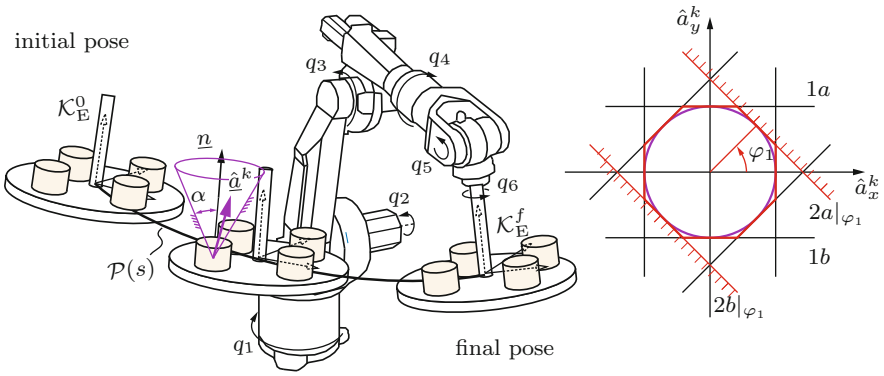

Fig. 1.7 Generalized waiter-motion with no-sliding constraints

an initial pose $\mathcal{K}_{\mathrm{E}}^{0}$ to a final pose $\mathcal{K}_{\mathrm{E}}^{f}$ as fast as possible such that objects placed on it do not slide (see Fig. 1.7). The problem is solvable in closed form for the case of one single glass, but leads to a yet unsolved complex problem for the case of few glasses placed at different positions on the tablet.

The task considered here is the computation of the fastest motion along a prescribed spatial path given as a spatial interpolation of key poses of $\mathcal{K}_{\mathrm{E}}$. One set of constraints is given as limits in the joint velocities and accelerations in the form

$$\begin{aligned} \underline{\dot{q}}^{\min} \le \underline{\dot{q}} \le \underline{\dot{q}}^{\max} \\ \underline{\ddot{q}}^{\min} \le \underline{\ddot{q}} \le \underline{\ddot{q}}^{\max} \end{aligned} \tag{1.29}$$

with $\dot{q}_i^{\min}$, $\dot{q}_i^{\max}$, $\ddot{q}_i^{\min}$ and $\ddot{q}_i^{\min}$ constant. These values are typically provided by the manufacturer and are usually pre-programmed in the robot controller as soft-limits.

A second set of constraints is given by the sticking ('no sliding') condition for every object k on the tablet

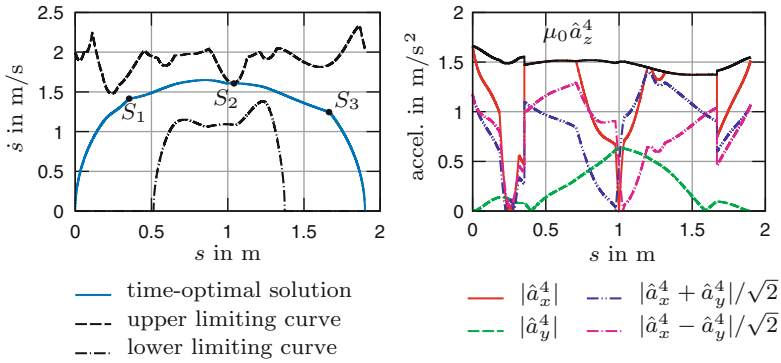

Fig. 1.8 Optimized waiter-motion along given trajectory

$$\frac{\hat{\underline{a}}^k \cdot \underline{n}}{\|\hat{\underline{a}}^k\|_2} \geq \cos\alpha, \quad \text{with } \hat{\underline{a}}^k = \underline{a}^k + \underline{g}, \tag{1.30}$$

where $\underline{a}^k$ is the acceleration of object k and $\underline{g}$ is the gravity vector, $\underline{n}$ is the normal vector of the tablet plane, and $\mu_0 = \tan\alpha$ is the dry friction coefficient between plane and objects. These k additional dynamic constraints can be rewritten as

$$\sqrt{[\hat{a}_x^k]^2 + [\hat{a}_y^k]^2} \leq \mu_0 \hat{a}_z^k, \quad \text{with } \hat{\underline{a}}^k = {}_k\mathbf{J}_s\, \ddot{s} + {}_k\mathbf{J}_s'\, \dot{s}^2 - \mathbf{R}_k^{\mathrm{T}} \underline{g}, \tag{1.31}$$

where ${}_k\mathbf{J}_s$ is the Jacobian mapping the linear velocities $\dot{s}$ along the spatial path to the velocities of object k, and $\mathbf{R}_k$ is the transformation matrix from the inertial frame to the local coordinate frame of object k.

Clearly, equations of the form Eq. 1.31 are nonlinear in the unknowns $\ddot{s}$, which makes their treatment with the previous methods infeasible. However, it is possible to approximate these constraints by replacing the friction cone by a friction polyhedra (Fig. 1.7) given by the equations

$$\begin{aligned} &1) \qquad |\hat{a}_x^k| \leq \mu_0 \hat{a}_z^k \\ &2) \quad \left| -\frac{\hat{a}_x^k}{\tan(\varphi_i)} + \hat{a}_y^k \right| \leq \frac{\mu_0 \hat{a}_z^k}{\sin(\varphi_i)}, \end{aligned} \tag{1.32}$$

defined by the discretization angles $\varphi_i = \frac{i\pi}{2^{p-1}}$, with $i = 1, 2, ..., 2^{p-1} - 1$, for each $\hat{a}_z^k$. Note that this approximation can be arbitrarily refined by choosing a sufficiently large integer p.

Equation 1.32 together with Eq. 1.29 form a system of constraints that are linear in $\dot{s}^2$, so that simply connected admissible acceleration regions are granted. The solution for the case of four objects symmetrically distributed on the tablet and a friction pyramid approximation with $p = 4$ is shown in Fig. 1.8. The plot at the right shows the accelerations of the fourth glass ($k = 4$).

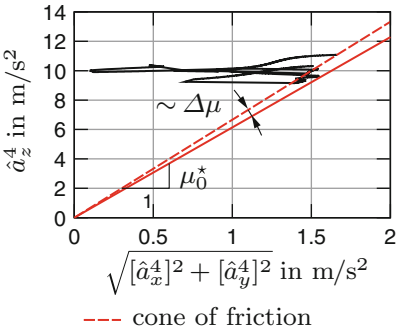

p	2^{p-1}	$\frac{\Delta\mu}{\mu_0}$ (%)	t_f (s)	CPU (s)
3	4	5.851	1.7000	5.906
4	8	5.850	1.7004	7.361
5	16	1.958	1.7033	11.230
6	32	0.483	1.7043	23.219
7	64	0.121	1.7046	65.183

Fig. 1.9 Delimitation of violations by relaxing the friction constraints

The small violations of the sticking condition are a consequence of the pyramid of friction approximation. They can be quantified by defining the friction correction $\Delta\mu$ (see Fig. 1.9), which is the smallest increase of the actual friction coefficient μ_0 that makes the computed motion feasible. As shown by the numerical experiments shown in Fig. 1.9, by increasing the integer p the accuracy of the constraint equations can be increased arbitrarily, although at expense of exponentially increasing CPU time.

1.5 Conclusions

This work extends classical fixed-geometry time-optimal path planning methods by (1) allowing for the consideration of sticking conditions and overall power consumption constraints, and (2) the allowing for general paths featuring smooth interpolation of angular acceleration as well as arbitrary multibody systems comprising multiple loops. The paper shows how the concept of motion interpolation as a kinetostatic transmission element allows for an efficient method to generate the transmission equations that lead to the formulation of the solution algorithm. The constraints can be straightforwardly constructed in terms of velocities, accelerations and forces at any place along the kinematical skeleton. The practical applicability of these extensions is illustrated by two applications from robotics and mining industry.

References

1. Bobrow JE, Dubowsky S, Gibson JS (1985) Time-optimal control of robotic manipulators along specified paths. Int J Robot Res 4(3):3–17
2. Dierckx P (1993) Curve and surface fitting with splines. Clarendon Press, Oxford
3. Kecskem'ethy A, Hiller M (1994) An object-oriented approach for an effective formulation of multibody dynamics. Comput Method Appl Mech Eng 115:287–314

4. Messner L, Gattringer H, Bremer H (2011) Generating speed, torque, and jerk limited trajectories along specified geometric paths in realtime. In: Proceedings of ROBO 2011, Pitsburgh
5. Pfeiffer F, Johanni R (1987) A concept for manipulator trajectory planning. IEEE J Robot Autom 3:115–123
6. Shiller Z, Lu HH (1990) Robust computation of path constrained time optimal motions. Proc IEEE Int Conf Robot Autom 1:144–149, Cincinnati
7. Shin KG, McKay ND (1985) Minimum-time control of robotic manipulators with geometric path constraints. IEEE Trans Autom Control 30(6):531–541
8. Tändl M, Kecskem'ethy A, Schneider M (2007) A design environment for industrial roller coasters. In: CD Proceedings of the ECCOMAS thematic conference on advances in computational multibody dynamics, Milano
9. Verscheure D, Demeulenaere B, Swevers J, De Schutter J, Diehl M (2009) Timeoptimal path tracking for robots: a convex optimization approach. IEEE Trans Autom Control 54 (10):2318–2327